Applied Mathematics and Computation 387 (2020) 124625

Contents lists available at ScienceDirect

Applied Mathematics and Computation

journal homepage: www.elsevier.com/locate/amc

Analysis of the parareal method with spectral deferred correction method for the Stokes/Darcy equations☆

Dandan Xue, Yanren Hou*, Wenjia Liu

School of Mathematics and Statistics, Xi'an Jiaotong University, Xi'an, Shaanxi 710049, China

ARTICLE INFO

Article history:
Available online 17 September 2019

Keywords:
Time-dependent
Stokes/Darcy equations
Parareal
Spectral deferred correction

ABSTRACT

In this paper, we analyze a second-order numerical algorithm for the non-stationary mixed Stokes/Darcy equations with Beavers–Joseph–Saffman's interface condition. The scheme is based on a finite element method in space and the parareal method with spectral deferred correction in time. We present the unconditional stability and the optimal error estimate of the full-discrete scheme. Finally, some numerical experiments are given to verify the effectiveness.

1. Introduction

The parareal algorithm, first proposed in 2001 by Lions et al. [1], can parallelize the numerical simulation in time for the time dependent partial differential equations. Since then, the parareal method has been widely studied, such as its convergency and stability in [2–6], a clear present of the efficient scheduling of the tasks in [7] and some applications in [8–12]. In this paper, we use a variant of the parareal algorithm in [13,14], based on a parallel variation of the spectral deferred correction method (SDC). Hereinafter, we denote it as the Para/SDC algorithm for simplicity.

The SDC method was proposed for stiff ordinary differential equations in [15] and further developed in [16–18] and the references therein. The main advantage of SDC method is that one can use a lower order numerical method to get a numerical solution with higher order accuracy by solving a series of deferred correction equations during each time step. While this may lead to higher and higher computational cost when more and more iterative steps are adopted in each time step to achieve such higher accuracy. So the combination with the parareal method can effectively make up the defect by distributing the computational cost to different computational cores.

Due to various applications in science and engineering, the coupling of incompressible flow and porous media flow has been widely studied in the past decades. We study the non-stationary mixed Stokes/Darcy model for the coupled fluid flow and porous media flow, which are coupled with certain transmission conditions on the interface. There is an extensive literature on the numerical methods for the mixed Stokes/Darcy model, see [19–32] and the references therein. In this paper, we present a second-order Para/SDC algorithm for the non-stationary mixed Stokes/Darcy model and give its numerical stability and the optimal error estimation.

The remainder of this paper is organized as follows. In Section 2, we introduce the non-stationary mixed Stokes/Darcy model. In Section 3, the full details of both the SDC algorithm and the Para/SDC algorithm are described. We present the

☆ Subsidized by NSFC (Grant no. 11971378 & 11571274).

* Corresponding author.
E-mail addresses: dandanxue@stu.xjtu.edu.cn (D. Xue), yrhou@mail.xjtu.edu.cn (Y. Hou), xjlwj99@stu.xjtu.edu.cn (W. Liu).

https://doi.org/10.1016/j.amc.2019.124625
0096-3003/

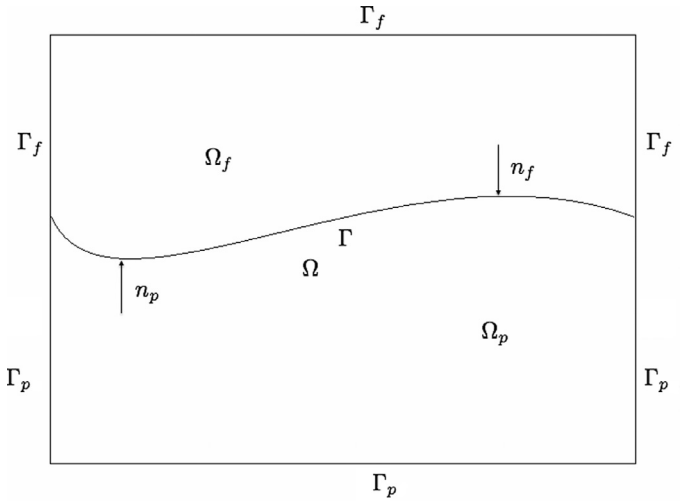

Fig. 1. The global domain Ω consisting of the fluid region Ω_f and the porous media region Ω_p separated by the interface Γ.

unconditional stability of the Para/SDC algorithm in Section 4 and the optimal error estimates in Section 5. Numerical experiments are reported in Section 6 to verify the analysis results and the advantage of our algorithm, followed by conclusions in Section 7.

2. The mixed Stokes/Darcy model

Let us consider the non-stationary mixed model of the Stokes equations and the Darcy equations in a bounded domain $\Omega \subset \mathbb{R}^d$ $(d = 2 \text{ or } 3)$, which consists of a fluid region Ω_f, a porous media region Ω_p and the interface $\Gamma = \overline{\Omega}_f \cap \overline{\Omega}_p$. Denote by $\Gamma_f = \partial\Omega_f \backslash \Gamma$, $\Gamma_p = \partial\Omega_p \backslash \Gamma$, $\boldsymbol{n}_f$ and $\boldsymbol{n}_p$ the unit outward normal vectors on $\partial\Omega_f$ and $\partial\Omega_p$, $\boldsymbol{\tau}_i$, $i = 1, \ldots, d-1$, the unit tangential vectors on the interface Γ, respectively. Furthermore, it is obvious that $\boldsymbol{n}_p = -\boldsymbol{n}_f$ on Γ. See Fig. 1 for a sketch.

Let $T > 0$ be a finite time. The fluid velocity and the kinematic pressure in the fluid region Ω_f are denoted by $\boldsymbol{u}$ and p, respectively, and φ is the piezometric head in the porous media region Ω_p. The partial differential equations governing the fluid flow and the porous media flow are

$$\begin{cases} \boldsymbol{u}_t - \nabla \cdot (2\nu \boldsymbol{D}(\boldsymbol{u}) - p\boldsymbol{I}) = \boldsymbol{f}_1, & \text{in } \Omega_f \times (0, T), \\ \nabla \cdot \boldsymbol{u} = 0, & \text{in } \Omega_f \times (0, T), \\ S_0 \varphi_t - \nabla \cdot (\boldsymbol{K} \nabla \varphi) = f_2, & \text{in } \Omega_p \times (0, T), \\ \boldsymbol{u}(\boldsymbol{x}, 0) = \boldsymbol{u}^0, & \text{in } \Omega_f, \\ \varphi(x, 0) = \varphi^0, & \text{in } \Omega_p, \end{cases} \tag{1}$$

where $\boldsymbol{D}(\boldsymbol{u})$ is the deformation rate tensor defined by $\boldsymbol{D}(\boldsymbol{u}) = \frac{1}{2}(\nabla \boldsymbol{u} + \nabla^T \boldsymbol{u})$, $\nu > 0$ is the kinematic viscosity, $\boldsymbol{I}$ is the $d \times d$ identity tensor, $\boldsymbol{f}_1$ is the external force acting on $\Omega_f \times [0, T]$, f_2 is the source term acting on $\Omega_p \times [0, T]$, S_0 is the specific mass storativity coefficient and $\boldsymbol{K}$ is the hydraulic conductivity tensor. We assume $\boldsymbol{K}$ is a symmetric positive definite matrix, $\boldsymbol{K} = \{K_{ij}\}_{i,j=1,\ldots,d}$, $K_{ij} \in L^\infty(\Omega_p)$, $K_{ij} > 0$, and it is uniformly bounded in Ω_p: there exist $k_{\min} > 0$ and $k_{\max} > 0$ such that

$$k_{min}|x|^2 \le \boldsymbol{K}x \cdot x \le k_{max}|x|^2 \quad a.e. \quad x \in \Omega_p. \tag{2}$$

The Eqs. (1) are completed by the boundary conditions stated in (4) and the following interface conditions along Γ:

$$\begin{aligned} &\boldsymbol{u} \cdot \boldsymbol{n}_f - \boldsymbol{K}\nabla\varphi \cdot \boldsymbol{n}_p = 0, && \text{on } \Gamma \times (0, T), \\ &p - \nu n_f \frac{\partial \boldsymbol{u}}{\partial \boldsymbol{n}_f} = g\varphi, && \text{on } \Gamma \times (0, T), \\ &-\nu \boldsymbol{\tau}_i \frac{\partial \boldsymbol{u}}{\partial \boldsymbol{n}_f} = \alpha \sqrt{\frac{\nu g}{\mathrm{tr}(\boldsymbol{K})}} (\boldsymbol{u} \cdot \boldsymbol{\tau}_i), \quad 1 \le i \le (d-1) && \text{on } \Gamma \times (0, T). \end{aligned} \tag{3}$$

Here g is the gravitational acceleration and α is a positive parameter depending on the properties of the porous medium. The first condition in (3) ensures the mass conservation across Γ, the second one states the balance of normal forces, and the third one means that the tangential components of the normal stress force is proportional to the tangential components of the fluid velocity, which is called the Beavers-Joseph-Saffman's (BJS) interface condition [33,34].

For simplicity, we assume that the fluid velocity and the piezometric head satisfy the homogenous Dirichlet boundary conditions on Γ_f and Γ_p, that is

$$\boldsymbol{u} = \boldsymbol{0} \text{ on } \Gamma_f \times (0, T), \quad \varphi = 0 \text{ on } \Gamma_p \times (0, T). \tag{4}$$

We define the following Hilbert spaces.

$$\boldsymbol{W}_f = \{\boldsymbol{v} \in (H^1(\Omega_f))^d : \boldsymbol{v} = \boldsymbol{0} \text{ on } \Gamma_f\}, \quad W_p = \{\psi \in H^1(\Omega_p) : \psi = 0 \text{ on } \Gamma_p\},$$
$$\boldsymbol{W} = \boldsymbol{W}_f \times W_p, \quad Q = L^2(\Omega_f),$$
$$\boldsymbol{V}_f = \{\boldsymbol{v} \in \boldsymbol{W}_f : \nabla \cdot \boldsymbol{v} = 0\}, \quad \boldsymbol{V} = \boldsymbol{V}_f \times W_p.$$

The space $\boldsymbol{W}$ is equipped with the following norms: for all $\underline{\boldsymbol{w}} = (\boldsymbol{u}, \varphi) \in \boldsymbol{W}$,

$$\|\underline{\boldsymbol{w}}\|_0 = \sqrt{(\boldsymbol{u}, \boldsymbol{u})_{\Omega_f} + gS_0(\varphi, \varphi)_{\Omega_p}},$$
$$\|\underline{\boldsymbol{w}}\|_W = \sqrt{2\nu(\boldsymbol{D}(\boldsymbol{u}), \boldsymbol{D}(\boldsymbol{u}))_{\Omega_f} + g(\boldsymbol{K}\nabla\varphi, \nabla\varphi)_{\Omega_p}}, \tag{5}$$

where $(\cdot, \cdot)_D$ refers to the scalar product in the corresponding domain D for $D = \Omega_f$ or Ω_p. Once again, for simplicity, we denote $\|\cdot\|_D = \|\cdot\|_{L^2(D)}$ hereinafter. In addition, if we take $\underline{\boldsymbol{w}} \in \boldsymbol{V}$, the norms for the space $\boldsymbol{V}$ are the same as that in space $\boldsymbol{W}$, denoted by $\|\underline{\boldsymbol{w}}\|_0$ and $\|\underline{\boldsymbol{w}}\|_V$.

Assume that

$$\boldsymbol{f}_1 \in L^2\big(0, T; L^2(\Omega_f)^d\big), \quad f_2 \in L^2\big(0, T; L^2(\Omega_p)\big), \quad \boldsymbol{K} \in L^\infty(\Omega_p)^{d\times d}.$$

Then the weak formulation of the non-stationary mixed Stokes and Darcy equations reads: find $\underline{\boldsymbol{w}} = (\boldsymbol{u}, \varphi) \in (L^2(0, T; \boldsymbol{W}_f) \cap L^\infty(0, T; L^2(\Omega_f))^d) \times (L^2(0, T; W_p) \cap L^\infty(0, T; L^2(\Omega_p)))$ and $p \in L^2(0, T; Q)$, such that

$$\begin{cases} [\underline{\boldsymbol{w}}_t, \underline{\boldsymbol{z}}] + a(\underline{\boldsymbol{w}}, \underline{\boldsymbol{z}}) + b(\underline{\boldsymbol{z}}, p) = (\boldsymbol{f}, \underline{\boldsymbol{z}}), & \forall\ \underline{\boldsymbol{z}} = (\boldsymbol{v}, \psi) \in \boldsymbol{W}, \\ b(\underline{\boldsymbol{w}}, q) = 0, & \forall\ q \in Q, \\ \underline{\boldsymbol{w}}(0) = \underline{\boldsymbol{w}}^0, \end{cases} \tag{6}$$

where

$$\begin{aligned} &[\underline{\boldsymbol{w}}_t, \underline{\boldsymbol{z}}] = (\boldsymbol{u}_t, \boldsymbol{v})_{\Omega_f} + gS_0(\varphi_t, \psi)_{\Omega_p}, \\ &a(\underline{\boldsymbol{w}}, \underline{\boldsymbol{z}}) = a_f(\boldsymbol{u}, \boldsymbol{v}) + a_p(\varphi, \psi) + a_\Gamma(\underline{\boldsymbol{w}}, \underline{\boldsymbol{z}}), \\ &a_f(\boldsymbol{u}, \boldsymbol{v}) = 2\nu(\boldsymbol{D}(\boldsymbol{u}), \boldsymbol{D}(\boldsymbol{v}))_{\Omega_f} + \sum_{i=1}^{d-1} \int_\Gamma \alpha \sqrt{\frac{\nu g}{\mathrm{tr}(\boldsymbol{K})}} (\boldsymbol{u} \cdot \boldsymbol{\tau}_i)(\boldsymbol{v} \cdot \boldsymbol{\tau}_i), \\ &a_p(\varphi, \psi) = g(\boldsymbol{K}\nabla\varphi, \nabla\psi)_{\Omega_p}, \\ &a_\Gamma(\underline{\boldsymbol{w}}, \underline{\boldsymbol{z}}) = g \int_\Gamma (\varphi \boldsymbol{v} \cdot n_f - \psi \boldsymbol{u} \cdot n_f), \\ &b(\underline{\boldsymbol{z}}, q) = -(q, \nabla \cdot \boldsymbol{v})_{\Omega_f}, \\ &(\boldsymbol{f}, \underline{\boldsymbol{z}}) = (\boldsymbol{f}_1, \boldsymbol{v})_{\Omega_f} + g(f_2, \psi)_{\Omega_p}. \end{aligned} \tag{7}$$

Furthermore, the interface term $a_\Gamma(\cdot, \cdot)$ in (7) is anti-symmetric,

$$a_\Gamma(\underline{\boldsymbol{w}}, \underline{\boldsymbol{z}}) = -a_\Gamma(\underline{\boldsymbol{z}}, \underline{\boldsymbol{w}}) \quad \text{and} \quad a_\Gamma(\underline{\boldsymbol{z}}, \underline{\boldsymbol{z}}) = 0, \quad \forall\ \underline{\boldsymbol{w}}, \underline{\boldsymbol{z}} \in \boldsymbol{W}. \tag{8}$$

Thanks to [21,29], there exists a constant $C_\Gamma > 0$ such that for all $\lambda > 0$,

$$|a_\Gamma(\underline{\boldsymbol{w}}, \underline{\boldsymbol{z}})| \le \lambda \|\underline{\boldsymbol{w}}\|_W^2 + \frac{C_\Gamma}{4\lambda} \|\underline{\boldsymbol{z}}\|_W^2, \quad \forall\ \underline{\boldsymbol{w}}, \underline{\boldsymbol{z}} \in \boldsymbol{W}. \tag{9}$$

In addition, assume the true solution $\underline{\boldsymbol{w}}(t) = (\boldsymbol{u}(t), \varphi(t))$ satisfies the following regularities

$$\begin{aligned} &\boldsymbol{u}(t) \in L^2(0, T; H^{k_1+1}(\Omega_f)^d), && \varphi(t) \in L^2(0, T; H^{k_2+1}(\Omega_p)), \\ &\boldsymbol{u}^0 \in H^{k_1+1}(\Omega_f)^d, && \varphi^0 \in H^{k_2+1}(\Omega_p), \\ &\boldsymbol{u}_t \in L^2(0, T; H^{k_1}(\Omega_f)^d), && \varphi_t \in L^2(0, T; H^{k_2}(\Omega_p)), \\ &\boldsymbol{u}_{tt} \in L^2(0, T; H^{k_1-1}(\Omega_f)^d), && \varphi_{tt} \in L^2(0, T; H^{k_2-1}(\Omega_p)), \\ &\boldsymbol{u}_{ttt} \in L^2(0, T; \boldsymbol{W}_f'), && \varphi_{ttt} \in L^2(0, T; W_p'), \end{aligned} \tag{10}$$

where $\boldsymbol{W}_f'$ and W_p' are the dual spaces of $\boldsymbol{W}_f$ and W_p respectively.

Let T_f^h and T_p^h be the regular triangulations of Ω_f and Ω_p, depending on a positive parameter h, made up of triangles if $d = 2$ or tetrahedra if $d = 3$. And we assume the triangulation $T^h = T_f^h \bigcup T_p^h$ of the global domain $\overline{\Omega}$ is quasi-uniform and compatible on the interface Γ. Let $\boldsymbol{W}_h = \boldsymbol{W}_{fh} \times W_{ph} \subset \boldsymbol{W}$ and $Q_h \subset Q$ denote the finite element spaces based on the above triangulations. Let $k_1 \ge 1$, $k_2 \ge 1$ and $k_3 \ge 1$ be three integers. The spaces $\boldsymbol{W}_{fh}$, W_{ph} and Q_h are chosen to be the finite element spaces with the k_1, k_2 and k_3 order accuracy, respectively. Furthermore, we assume $(\boldsymbol{W}_{fh}, Q_h)$ satisfies the well-known discrete inf-sup condition: there exists a positive constant β, independent of h such that

$$\inf_{q \in Q_h} \sup_{\underline{\boldsymbol{z}} \in \boldsymbol{W}_h} \frac{b(\underline{\boldsymbol{z}}, q)}{\|\underline{\boldsymbol{z}}\|_W \|q\|_{\Omega_f}} \ge \beta. \tag{11}$$

And we introduce a finite element space $\boldsymbol{V}_{fh} \subset \boldsymbol{W}_{fh}$ defined on Ω_f as

$$\boldsymbol{V}_{fh} = \{\boldsymbol{v}_h \in \boldsymbol{W}_{fh} : (\nabla \cdot \boldsymbol{v}_h, q_h)_{\Omega_f} = 0, \ \forall q_h \in Q_h\}, \quad \boldsymbol{V}_h = \boldsymbol{V}_{fh} \times W_{ph}.$$

Since the bilinear form $a(\cdot, \cdot)$ is continuous and elliptic on $\boldsymbol{V}_h$, we define a elliptic projection $P_h^w : \underline{\boldsymbol{w}} \in \boldsymbol{V} \mapsto P_h^w \underline{\boldsymbol{w}} \in \boldsymbol{V}_h$ satisfying

$$a(P_h^w \underline{\boldsymbol{w}}, \underline{\boldsymbol{z}}_h) = a(\underline{\boldsymbol{w}}, \underline{\boldsymbol{z}}_h), \ \forall \underline{\boldsymbol{z}}_h \in \boldsymbol{V}_h.$$

From the inf-sup condition (11), we get a projection operator $P_h^p : p \in Q \mapsto P_h^p p \in Q_h$ satisfying

$$b(\underline{\boldsymbol{z}}_h, P_h^p p) = b(\underline{\boldsymbol{z}}_h, p), \ \forall \underline{\boldsymbol{z}}_h \in \boldsymbol{V}_h.$$

Obviously, we can get for any $\underline{\boldsymbol{w}} \in \boldsymbol{V}$ and $p \in Q$,

$$\begin{aligned} &a(\underline{\boldsymbol{w}} - P_h^w \underline{\boldsymbol{w}}, \underline{\boldsymbol{z}}_h) = b(\underline{\boldsymbol{z}}_h, p - P_h^p p) = 0, \quad \forall \underline{\boldsymbol{z}}_h \in \boldsymbol{V}_h, \\ &b(\underline{\boldsymbol{w}} - P_h^w \underline{\boldsymbol{w}}, q_h) = 0, \quad \forall q_h \in Q_h. \end{aligned} \tag{12}$$

In addition, if we assume $\underline{\boldsymbol{w}}(t) \in H^l(\Omega_f)^d \times H^s(\Omega_p)$ and $p(t) \in H^r(\Omega_f)$ ($l, s > 1$, $r > 0$), are the solutions of (1)-(4), then the projection $\left(P_h^w \underline{\boldsymbol{w}}(t), P_h^p p(t)\right)$ of $(\underline{\boldsymbol{w}}(t), p(t))$ satisfies the following approximation properties :

$$\begin{aligned} &\|\underline{\boldsymbol{w}}(t) - P_h^w \underline{\boldsymbol{w}}(t)\|_0 \le Ch^l \|\boldsymbol{u}(t)\|_{H^l(\Omega_f)} + Ch^s \|\varphi(t)\|_{H^s(\Omega_p)}, \\ &\|\underline{\boldsymbol{w}}(t) - P_h^w \underline{\boldsymbol{w}}(t)\|_V \le Ch^{l-1} \|\boldsymbol{u}(t)\|_{H^l(\Omega_f)} + Ch^{s-1} \|\varphi(t)\|_{H^s(\Omega_p)}, \\ &\|p(t) - P_h^p p(t))\|_{L^2(\Omega_f)} \le Ch^r \|p(t)\|_{H^r(\Omega_f)}, \end{aligned} \tag{13}$$

where C is a positive constant which is different in different places but independent of mesh size and time step.

3. The para/SDC algorithm

The Para/SDC algorithm to be considered is a variant of the parareal method, so we first introduce the SDC method and then the parareal method. Let us consider the initial value problem

$$\begin{cases} \boldsymbol{w}'(t) = \boldsymbol{f}(t, \boldsymbol{w}(t)), \quad t \in [0, T], \\ \boldsymbol{w}(0) = \boldsymbol{w}^0, \end{cases} \tag{14}$$

where $\boldsymbol{w}(t)$, $\boldsymbol{w}^0 \in \mathbb{C}^d$ and $\boldsymbol{f} : \mathbb{R} \times \mathbb{C}^d \to \mathbb{C}^d$.

3.1. The spectral deferred correction algorithm

We present a SDC algorithm based on the first-order Euler method for the system (14). The corresponding Picard integral form of the solution to (14) is

$$\boldsymbol{w}(t) = \boldsymbol{w}^0 + \int_0^t \boldsymbol{f}(\tau, \boldsymbol{w}(\tau)) d\tau. \tag{15}$$

Suppose that we have gotten an approximate solution $\boldsymbol{w}_1(t)$ to (15). If we define the error $\boldsymbol{\delta}(t) = \boldsymbol{w}(t) - \boldsymbol{w}_1(t)$, we can construct a correction equation

$$\boldsymbol{\delta}(t) = \int_0^t \left(\boldsymbol{f}(\tau, \boldsymbol{w}_1(\tau) + \boldsymbol{\delta}(\tau)) - \boldsymbol{f}(\tau, \boldsymbol{w}_1(\tau))\right) d\tau + E(t, \boldsymbol{w}_1(t)), \tag{16}$$

where $E(t, \boldsymbol{w}_1(t))$ is the residual function denoted by

$$E(t, \boldsymbol{w}_1(t)) = \boldsymbol{w}^0 + \int_0^t \boldsymbol{f}(\tau, \boldsymbol{w}_1(\tau)) d\tau - \boldsymbol{w}_1(t).$$

In the numerical discretization, the time interval $[0, T]$ is divided into N subintervals $[t^n, t^{n+1}]$ by choosing points $t^n = n\Delta t = n\frac{T}{N}$ for $n = 0, \ldots, N$ with $0 = t^0 < t^1 < \ldots < t^N = T$. Let $\boldsymbol{w}_i^n$ denote the numerical approximations to $\boldsymbol{w}(t^n)$. Assume that a sequence of the approximate solutions $\boldsymbol{w}_1^{n+1}$ are firstly obtained by the first-order backward Euler method, i.e.

$$\boldsymbol{w}_1^{n+1} = \boldsymbol{w}_1^n + \Delta t \boldsymbol{f}(t^{n+1}, \boldsymbol{w}_1^{n+1}). \tag{17}$$

We approximate (16) by a simple discretization that resembles backward Euler, leading to the implicit approximation of the correction equation

$$\boldsymbol{\delta}_i^{n+1} = \boldsymbol{\delta}_i^n + \Delta t \left(\boldsymbol{f}(t^{n+1}, \boldsymbol{w}_i^{n+1} + \boldsymbol{\delta}_i^{n+1}) - \boldsymbol{f}(t^{n+1}, \boldsymbol{w}_i^{n+1})\right) + E(t^{n+1}, \boldsymbol{w}_i^{n+1}) - E(t^n, \boldsymbol{w}_i^n).$$

Then the corrected solution $\boldsymbol{w}_{i+1}^{n+1} = \boldsymbol{w}_i^{n+1} + \boldsymbol{\delta}_i^{n+1}$ satisfies the following equation

$$\boldsymbol{w}_{i+1}^{n+1} = \boldsymbol{w}_{i+1}^{n} + \Delta t\left(\boldsymbol{f}(t^{n+1}, \boldsymbol{w}_{i+1}^{n+1}) - \boldsymbol{f}(t^{n+1}, \boldsymbol{w}_i^{n+1})\right) + I_n^{n+1}(\boldsymbol{w}_i), \tag{18}$$

where $I_n^{n+1}(\boldsymbol{w}_i)$ is the numerical quadrature approximation to

$$\int_{t^n}^{t^{n+1}} \boldsymbol{f}(\tau, \boldsymbol{w}_i(\tau))d\tau. \tag{19}$$

As long as the approximation of (19) is accurate, each iteration of the correction Eq. (18) will increase the accuracy of the approximate solution for one order, as we use the first-order method to approximate the correction equation.

In [17], the comparisons with other existing methods, such as high-order linear multi-step method and Runge-Kutta method, show that the higher-order SDC method is more accurate and easier to construct. Nevertheless, the SDC method still has a disadvantage: the large computation cost. As mentioned earlier, the premise of the high-order SDC method is the accuracy of the numerical approximation of (19). While the more accuracy of the numerical quadrature approximation is required, the more nodes and therefore more corrections are needed in each time step $[t^n, t^{n+1}]$. Obviously, this leads to an increase in the computational cost. An effective way to deal with the problem is the combination with the parareal method, so that the computational cost can be distributed to a set of computational cores. This is also the motivation of the so-called Para/SDC scheme to be constructed.

3.2. The para/SDC algorithm

For the parareal method, the time interval [0, T] needs to be divided into N subintervals $[t^n, t^{n+1}] = [t^n, t^n + \Delta t]$ and the subintervals are assigned to different processors. For simplicity, denote the processors P_1 through P_N. Following [13,14], we give two numerical approximation methods denoted by $\mathcal{G}$ and $\mathcal{F}$ propagator. For the sake of efficiency of the parareal method, $\mathcal{G}$ is computationally less expensive than $\mathcal{F}$. Futhermore, we denote by $\mathcal{G}(t^{n+1}, t^n, \hat{\boldsymbol{w}})$ and $\mathcal{F}(t^{n+1}, t^n, \hat{\boldsymbol{w}})$ the numerical solutions at time t^{n+1} with the initial value $\hat{\boldsymbol{w}}$ by using $\mathcal{G}$ and $\mathcal{F}$ respectively.

In the parareal method, $\mathcal{G}$ is used to compute a provisional solution at all nodes sequentially, i.e.,

$$\boldsymbol{w}_1^{n+1} = \mathcal{G}(t^{n+1}, t^n, \boldsymbol{w}_1^n), \ \ n = 0, \ldots, N-1.$$

As soon as each processor P_n obtains the initial value $\boldsymbol{w}_1^n$, they can compute a more accurate approximate solution $\mathcal{F}(t^{n+1}, t^n, \boldsymbol{w}_1^n)$ in parallel. Then the serial correction step takes the form

$$\boldsymbol{w}_2^{n+1} = \mathcal{G}(t^{n+1}, t^n, \boldsymbol{w}_2^n) + \mathcal{F}(t^{n+1}, t^n, \boldsymbol{w}_1^n) - \mathcal{G}(t^{n+1}, t^n, \boldsymbol{w}_1^n). \tag{20}$$

After the discussion on the parareal method, we focus on the Para/SDC method in the remainder of this section. In [16], the Para/SDC method selects some SDC sweeps as $\mathcal{F}$ propagator. In this paper, we apply the backward Euler method as $\mathcal{G}$, and a SDC sweep like (18) as $\mathcal{F}$.

In addition, in order to construct a second-order scheme, we apply the trapezoid formula to approximate (19), i.e.

$$I_n^{n+1}(\boldsymbol{w}_1) = \frac{1}{2}\Delta t\left(\boldsymbol{f}(t^{n+1}, \boldsymbol{w}_1^{n+1}) + \boldsymbol{f}(t^n, \boldsymbol{w}_1^n)\right), \ \ n = 0, \ldots, N-1. \tag{21}$$

Therefore, we just use two quadrature points to approximate the integral (19). Using (21), we rewrite (18) with the initial value $\boldsymbol{w}_1^n$ to get the approximation $\mathcal{F}(t_{n+1}, t_n, \boldsymbol{w}_1^n)$ in parallel, that is

$$\begin{aligned} \mathcal{F}(t_{n+1}, t_n, \boldsymbol{w}_1^n) \quad &:= \ \boldsymbol{\lambda}^{n+1} = \boldsymbol{w}_1^n + \Delta t\left(\boldsymbol{f}(t^{n+1}, \boldsymbol{\lambda}^{n+1}) - \boldsymbol{f}(t^{n+1}, \boldsymbol{w}_1^{n+1})\right) + I_n^{n+1}(\boldsymbol{w}_1), \\ &= \ \boldsymbol{w}_1^n + \Delta t\boldsymbol{f}(t^{n+1}, \boldsymbol{\lambda}^{n+1}) - \frac{\Delta t}{2}\boldsymbol{f}(t^{n+1}, \boldsymbol{w}_1^{n+1}) + \frac{\Delta t}{2}\boldsymbol{f}(t^n, \boldsymbol{w}_1^n). \end{aligned} \tag{22}$$

Next, we describe our Para/SDC algorithm for the system (14).

Algorithm 1. (The Para/SDC algorithm)

1. Compute $\boldsymbol{w}_1^{n+1}$ by using the first-order backward Euler method $\mathcal{G}$ in serial

$$\boldsymbol{w}_1^{n+1} = \mathcal{G}(t_{n+1}, t_n, \boldsymbol{w}_1^n) = \boldsymbol{w}_1^n + \Delta t\boldsymbol{f}(t^{n+1}, \boldsymbol{w}_1^{n+1}), \tag{23}$$

   for $n = 0, \ldots, N-1$ starting with $\boldsymbol{w}_1^0 = \boldsymbol{w}^0$.
2. The processors use (22) to compute $\mathcal{F}(t_{n+1}, t_n, \boldsymbol{w}_1^n)$ for $n = 0, \ldots, N-1$ in parallel.
3. Compute the final solution $\boldsymbol{w}_2^{n+1}$ by the following serial correction step

$$\begin{cases} \boldsymbol{w}_2^{n+1} = \mathcal{G}(t_{n+1}, t_n, \boldsymbol{w}_2^n) + \mathcal{F}(t_{n+1}, t_n, \boldsymbol{w}_1^n) - \mathcal{G}(t_{n+1}, t_n, \boldsymbol{w}_1^n), \\ \boldsymbol{w}_2^0 = \boldsymbol{w}^0. \end{cases} \tag{24}$$

In order to test the parallel efficiency of the parareal method, we define a parallel speedup, the ratio of the serial to the parallel cost. In the Para/SDC algorithm (23), (24), both $\mathcal{G}$ and $\mathcal{F}$ use the same time step $\Delta t = T/N$ and we denote the computational cost of $\mathcal{G}$ and $\mathcal{F}$ for one time step as Υ_G and Υ_F, respectively. What's more, there are N processors to compute $\mathcal{F}$ concurrently and there is only one iteration of the correction step. Generally, we omit the communication time between the processors and assume that each processor is identical. Following [13] and [14], the total computational cost of the K iterations of the pipelined version of the Para/SDC method using N processors is $N\Upsilon_G + K(\Upsilon_F + \Upsilon_G)$. Furthermore, for the serial SDC scheme, the total computational cost is $N(K\Upsilon_F + \Upsilon_G)$. Hence the speedup of the Para/SDC algorithm (23), (24) is $\frac{N\Upsilon_G + N\Upsilon_F}{(N+1)\Upsilon_G + \Upsilon_F}$.

Using the finite element method for the spatial discretization, we can obtain the full-discrete second-order scheme of the Para/SDC algorithm for the non-stationary Stokes/Darcy model.

Algorithm 2. (The Para/SDC algorithm for the Stokes/Darcy model)

1. Using the backward Euler method to get $\mathcal{G}(t_{n+1}, t_n, \boldsymbol{w}_{1,h}^n)$ for $n = 0, \ldots, N-1$ sequentially, which means that find $(\underline{\boldsymbol{w}}_{1,h}^{n+1}, p_{1,h}^{n+1}) \in \boldsymbol{W}_h \times Q_h$ such that for all $\underline{\boldsymbol{z}}_h \in \boldsymbol{W}_h$ and $q_h \in Q_h$,

$$\begin{cases} \left[\frac{\underline{\boldsymbol{w}}_{1,h}^{n+1} - \underline{\boldsymbol{w}}_{1,h}^{n}}{\Delta t}, \underline{\boldsymbol{z}}_h\right] + a\left(\underline{\boldsymbol{w}}_{1,h}^{n+1}, \underline{\boldsymbol{z}}_h\right) + b\left(\underline{\boldsymbol{z}}_h, p_{1,h}^{n+1}\right) = (\boldsymbol{f}^{n+1}, \underline{\boldsymbol{z}}_h), \\ b(\underline{\boldsymbol{w}}_{1,h}^{n+1}, q_h) = 0, \\ \underline{\boldsymbol{w}}_{1,h}^{0} = P_h^w \underline{\boldsymbol{w}}^0. \end{cases} \tag{25}$$

2. Using (22) to compute $\mathcal{F}(t_{n+1}, t_n, \boldsymbol{w}_{1,h}^n)$ for $n = 0, \ldots, N-1$ in parallel. Take processor P_n for example: find $(\underline{\boldsymbol{\lambda}}_h^{n+1}, p_{\lambda,h}^{n+1}) \in \boldsymbol{W}_h \times Q_h$ such that for all $\underline{\boldsymbol{z}}_h \in \boldsymbol{W}_h$ and $q_h \in Q_h$,

$$\begin{cases} \left[\frac{\underline{\boldsymbol{\lambda}}_h^{n+1} - \underline{\boldsymbol{w}}_{1,h}^{n}}{\Delta t}, \underline{\boldsymbol{z}}_h\right] + a\left(\underline{\boldsymbol{\lambda}}_h^{n+1}, \underline{\boldsymbol{z}}_h\right) + b\left(\underline{\boldsymbol{z}}_h, p_{\lambda,h}^{n+1}\right) \\ \quad = a\left(\frac{\underline{\boldsymbol{w}}_{1,h}^{n+1} - \underline{\boldsymbol{w}}_{1,h}^{n}}{2}, \underline{\boldsymbol{z}}_h\right) + b\left(\underline{\boldsymbol{z}}_h, \frac{p_{1,h}^{n+1} - p_{1,h}^{n}}{2}\right) + \left(\frac{\boldsymbol{f}^{n+1} + \boldsymbol{f}^{n}}{2}, \underline{\boldsymbol{z}}_h\right), \\ b\left(\underline{\boldsymbol{\lambda}}_h^{n+1}, q_h\right) = 0. \end{cases} \tag{26}$$

3. Compute $\mathcal{G}(t_{n+1}, t_n, \boldsymbol{w}_{2,h}^n)$ for $n = 0, \ldots, N-1$ sequentially as (25): find $(\underline{\boldsymbol{w}}_h^{n+1}, p_h^{n+1}) \in \boldsymbol{W}_h \times Q_h$ such that for all $\underline{\boldsymbol{z}}_h \in \boldsymbol{W}_h$ and $q_h \in Q_h$,

$$\begin{cases} \left[\frac{\underline{\boldsymbol{w}}_h^{n+1} - \underline{\boldsymbol{w}}_{2,h}^{n}}{\Delta t}, \underline{\boldsymbol{z}}_h\right] + a\left(\underline{\boldsymbol{w}}_h^{n+1}, \underline{\boldsymbol{z}}_h\right) + b\left(\underline{\boldsymbol{z}}_h, p_h^{n+1}\right) = (\boldsymbol{f}^{n+1}, \underline{\boldsymbol{z}}_h), \\ b(\underline{\boldsymbol{w}}_h^{n+1}, q_h) = 0, \\ \underline{\boldsymbol{w}}_h^{0} = P_h^w \underline{\boldsymbol{w}}^0. \end{cases} \tag{27}$$

Then we get the final approximate solution $(\underline{\boldsymbol{w}}_{2,h}^{n+1}, p_{2,h}^{n+1})$ from (24):

$$\begin{cases} \underline{\boldsymbol{w}}_{2,h}^{n+1} = \underline{\boldsymbol{w}}_h^{n+1} + \underline{\boldsymbol{\lambda}}_h^{n+1} - \underline{\boldsymbol{w}}_{1,h}^{n+1}, \\ p_{2,h}^{n+1} = p_h^{n+1} + p_{\lambda,h}^{n+1} - p_{1,h}^{n+1}. \end{cases} \tag{28}$$

For later analysis, we rewrite (25)–(28) in the following compact form: find $(\underline{\boldsymbol{w}}_{2,h}^{n+1}, p_{2,h}^{n+1}) \in \boldsymbol{W}_h \times Q_h$ such that for all $\underline{\boldsymbol{z}}_h \in \boldsymbol{W}_h$ and $q_h \in Q_h$,

$$\begin{cases} \left[\frac{\underline{\boldsymbol{w}}_{2,h}^{n+1} - \underline{\boldsymbol{w}}_{2,h}^{n}}{\Delta t}, \underline{\boldsymbol{z}}_h\right] + a\left(\underline{\boldsymbol{w}}_{2,h}^{n+1}, \underline{\boldsymbol{z}}_h\right) + b\left(\underline{\boldsymbol{z}}_h, p_{2,h}^{n+1}\right) \\ = \frac{1}{2}a\left(\underline{\boldsymbol{w}}_{1,h}^{n+1}, \underline{\boldsymbol{z}}_h\right) - \frac{1}{2}a\left(\underline{\boldsymbol{w}}_{1,h}^{n}, \underline{\boldsymbol{z}}_h\right) + \frac{1}{2}b\left(\underline{\boldsymbol{z}}_h, p_{1,h}^{n+1}\right) - \frac{1}{2}b\left(\underline{\boldsymbol{z}}_h, p_{1,h}^{n}\right) + \left(\frac{\boldsymbol{f}^{n+1} + \boldsymbol{f}^{n}}{2}, \underline{\boldsymbol{z}}_h\right), \\ b\left(\underline{\boldsymbol{w}}_{2,h}^{n+1}, q_h\right) = 0, \\ \underline{\boldsymbol{w}}_{2,h}^{0} = P_h^w \underline{\boldsymbol{w}}^0. \end{cases} \tag{29}$$

4. The stability of the para/SDC algorithm

To derive the stability of the Para/SDC algorithm, we need the stability of the first-order scheme (25). Since the unconditional stability of the scheme (25) has been proved in the previous work see [28], we just quote the results.

Lemma 4.1. *For any $1 \le m \le N$, the solution $\underline{\boldsymbol{w}}_{1,h}^m = (\boldsymbol{u}_{1,h}^m, \varphi_{1,h}^m)$ to (25) satisfies*

$$\|\underline{\boldsymbol{w}}_{1,h}^m\|_0^2 + \Delta t \sum_{n=0}^{m-1} \|\underline{\boldsymbol{w}}_{1,h}^{n+1}\|_W^2 \le \|\underline{\boldsymbol{w}}^0\|_0^2 + \frac{C}{\nu}\Delta t \sum_{n=0}^{m-1} \|\boldsymbol{f}_1^{n+1}\|_{\Omega_f}^2 + \frac{Cg}{k_{min}}\Delta t \sum_{n=0}^{m-1} \|f_2^{n+1}\|_{\Omega_p}^2. \tag{30}$$

Next, we will use the result of Lemma 4.1 to present the stability for the Algorithm 2.

Theorem 4.1. *If $\underline{\boldsymbol{w}}_{2,h}^m = (\boldsymbol{u}_{2,h}^m, \varphi_{2,h}^m)$ with $1 \le m \le N$ is the solution of Algorithm 2, it satisfies*

$$\|\underline{\boldsymbol{w}}_{2,h}^m\|_0^2 + \Delta t \sum_{n=0}^{m-1} \|\underline{\boldsymbol{w}}_{2,h}^{n+1}\|_W^2 \le C\left(\|\underline{\boldsymbol{w}}^0\|_0^2 + \frac{1}{\nu}\Delta t \sum_{n=0}^{m} \|\boldsymbol{f}_1^{n}\|_{\Omega_f}^2 + \frac{g}{k_{min}}\Delta t \sum_{n=0}^{m} \|f_2^{n}\|_{\Omega_p}^2\right). \tag{31}$$

Proof. Setting $\underline{z}_h = 2\Delta t \underline{\boldsymbol{w}}_{2,h}^{n+1}$ and $q_h = p_{2,h}^{n+1}$ in (29), we have

$$\begin{aligned}
&\left(\|\underline{\boldsymbol{w}}_{2,h}^{n+1}\|_0^2 - \|\underline{\boldsymbol{w}}_{2,h}^{n}\|_0^2 + \|\underline{\boldsymbol{w}}_{2,h}^{n+1} - \underline{\boldsymbol{w}}_{2,h}^{n}\|_0^2\right) + 2\Delta t\|\underline{\boldsymbol{w}}_{2,h}^{n+1}\|_W^2 + 2\Delta t \sum_{i=1}^{d-1} \alpha \sqrt{\frac{\nu g}{\mathrm{tr}(\boldsymbol{K})}} \|\boldsymbol{w}_{2,h}^{n+1} \cdot \tau_i\|_{L^2(\Gamma)}^2 \\
&= \Delta t a\left(\underline{\boldsymbol{w}}_{1,h}^{n+1}, \underline{\boldsymbol{w}}_{2,h}^{n+1}\right) - \Delta t a\left(\underline{\boldsymbol{w}}_{1,h}^{n}, \underline{\boldsymbol{w}}_{2,h}^{n+1}\right) + 2\Delta t\left(\frac{\boldsymbol{f}^{n+1} + \boldsymbol{f}^n}{2}, \underline{\boldsymbol{w}}_{2,h}^{n+1}\right).
\end{aligned} \tag{32}$$

We bound each term on the right hand side of (32) as follows. Using the Poincare, Young's inequalities, (2) and (9), we get

$$\begin{aligned}
I &= \Delta t a(\underline{\boldsymbol{w}}_{1,h}^{n+1}, \underline{\boldsymbol{w}}_{2,h}^{n+1}) - \Delta t a(\underline{\boldsymbol{w}}_{1,h}^{n}, \underline{\boldsymbol{w}}_{2,h}^{n+1}) \\
&\le 2\varepsilon\Delta t\|\underline{\boldsymbol{w}}_{2,h}^{n+1}\|_W^2 + \Delta t \sum_{i=1}^{d-1} \alpha \sqrt{\frac{\nu g}{\mathrm{tr}(\boldsymbol{K})}} \|\boldsymbol{u}_{2,h}^{n+1} \cdot \tau_i\|_{L^2(\Gamma)}^2 + \frac{C}{\varepsilon}\Delta t\|\underline{\boldsymbol{w}}_{1,h}^{n+1}\|_W^2 + \frac{C}{\varepsilon}\Delta t\|\underline{\boldsymbol{w}}_{1,h}^{n}\|_W^2, \\
II &= 2\Delta t\left(\frac{\boldsymbol{f}^{n+1} + \boldsymbol{f}^n}{2}, \underline{\boldsymbol{w}}_{2,h}^{n+1}\right) = 2\Delta t\left(\frac{\boldsymbol{f}_1^{n+1} + \boldsymbol{f}_1^n}{2}, \boldsymbol{u}_{2,h}^{n+1}\right)_{\Omega_f} + 2\Delta t g\left(\frac{f_2^{n+1} + f_2^n}{2}, \varphi_{2,h}^{n+1}\right)_{\Omega_p} \\
&\le \varepsilon\Delta t\|\underline{\boldsymbol{w}}_{2,h}^{n+1}\|_W^2 + \frac{C}{\varepsilon\nu}\Delta t\|\frac{\boldsymbol{f}_1^{n+1} + \boldsymbol{f}_1^n}{2}\|_{\Omega_f}^2 + \frac{Cg}{\varepsilon k_{min}}\Delta t\|\frac{f_2^{n+1} + f_2^n}{2}\|_{\Omega_p}^2.
\end{aligned}$$

Combining the above estimates with (32) and setting $\varepsilon = 1/3$, we have

$$\begin{aligned}
&\|\underline{\boldsymbol{w}}_{2,h}^{n+1}\|_0^2 - \|\underline{\boldsymbol{w}}_{2,h}^{n}\|_0^2 + \|\underline{\boldsymbol{w}}_{2,h}^{n+1} - \underline{\boldsymbol{w}}_{2,h}^{n}\|_0^2 + \Delta t\|\underline{\boldsymbol{w}}_{2,h}^{n+1}\|_W^2 \\
&\le C\Delta t\|\underline{\boldsymbol{w}}_{1,h}^{n+1}\|_W^2 + C\Delta t\|\underline{\boldsymbol{w}}_{1,h}^{n}\|_W^2 + \frac{C}{\nu}\Delta t\left\|\frac{\boldsymbol{f}_1^{n+1} + \boldsymbol{f}_1^n}{2}\right\|_{\Omega_f}^2 + \frac{Cg}{k_{min}}\Delta t\left\|\frac{f_2^{n+1} + f_2^n}{2}\right\|_{\Omega_p}^2.
\end{aligned} \tag{33}$$

Summing (33) from $n = 0$ to $n = m - 1$ yields

$$\|\underline{\boldsymbol{w}}_{2,h}^{m}\|_0^2 + \Delta t \sum_{n=0}^{m-1} \|\underline{\boldsymbol{w}}_{2,h}^{n+1}\|_W^2 \le \|\underline{\boldsymbol{w}}_{2,h}^{0}\|_0^2 + C\Delta t \sum_{n=0}^{m} \|\underline{\boldsymbol{w}}_{1,h}^{n}\|_W^2 + \frac{C}{\nu}\Delta t \sum_{n=0}^{m} \|\boldsymbol{f}_1^{n}\|_{\Omega_f}^2 + \frac{Cg}{k_{min}}\Delta t \sum_{n=0}^{m} \|f_2^{n}\|_{\Omega_p}^2.$$

Combining $\|\underline{\boldsymbol{w}}_{2,h}^0\|_0 = \|P_h^w \underline{\boldsymbol{w}}^0\|_0 \le \|\underline{\boldsymbol{w}}^0\|_0$ and (30), we arrive at (31). □

5. The error analysis of the para/SDC algorithm

Firstly, the errors between the numerical solutions and the exact ones, can be decomposed into the numerical errors and the approximation errors as follows:

$$\begin{aligned}
&\underline{\boldsymbol{w}}_{k,h}^m - \underline{\boldsymbol{w}}^m = \underline{\boldsymbol{w}}_{k,h}^m - \tilde{\underline{\boldsymbol{w}}}^m - (\underline{\boldsymbol{w}}^m - \tilde{\underline{\boldsymbol{w}}}^m) := \underline{\boldsymbol{e}}_k^m - \underline{\boldsymbol{\xi}}^m, \ \ k = 1, 2, \\
&p_{k,h}^m - p^m = (p_{k,h}^m - \tilde{p}^m) - (p^m - \tilde{p}^m) := \varepsilon_k^m - \eta^m, \ \ k = 1, 2.
\end{aligned} \tag{34}$$

Here $\tilde{\underline{\boldsymbol{w}}}^m = P_h^w \underline{\boldsymbol{w}}^m$ and $\tilde{p}^m = P_h^p p^m$. Obviously, from (10) and (13), we have

$$\begin{aligned}
&\|\underline{\boldsymbol{\xi}}^m\|_0 \le C(h^{k_1+1}\|\boldsymbol{u}^m\|_{H^{k_1+1}(\Omega_f)} + h^{k_2+1}\|\varphi^m\|_{H^{k_2+1}(\Omega_p)}), \\
&\|\underline{\boldsymbol{\xi}}^m\|_V \le C(h^{k_1}\|\boldsymbol{u}^m\|_{H^{k_1+1}(\Omega_f)} + h^{k_2}\|\varphi^m\|_{H^{k_2+1}(\Omega_p)}).
\end{aligned}$$

Let $\boldsymbol{W}'$ be the dual space of $\boldsymbol{W}$ and let $\|\cdot\|_{W'}$ denote the dual norm. As usual, we denote by $<.,.>$ the duality pair between the space $\boldsymbol{W}$ and $\boldsymbol{W}'$. Similarly, one can define the dual spaces of $\boldsymbol{V}$ and $\boldsymbol{V}_h$.

Lemma 5.1. *Denote* $\underline{\boldsymbol{\xi}}^m = (I - P_h^w)\underline{\boldsymbol{w}}^m := Q_h\underline{\boldsymbol{w}}^m,\ \forall \underline{\boldsymbol{w}}^m \in \boldsymbol{V}$. *We have*

$$\|\underline{\boldsymbol{\xi}}^m\|_{\boldsymbol{V}_h'} \le Ch^2\|\underline{\boldsymbol{\xi}}^m\|_V. \tag{35}$$

Proof. To prove (35), we consider the following problem: for any given $\boldsymbol{f} \in \boldsymbol{V}'$, find $\underline{\boldsymbol{w}} \in \boldsymbol{W}$ such that,

$$a(\underline{\boldsymbol{w}}, \underline{\boldsymbol{z}}) = <\boldsymbol{f}, \underline{\boldsymbol{z}}>, \quad \forall \underline{\boldsymbol{z}} \in \boldsymbol{V}.$$

The problem is well-posed since the bilinear form $a(\cdot,\cdot)$ is continuous and elliptic on $\boldsymbol{V}$. Furthermore, we can define a bounded linear operator A: $\boldsymbol{V} \mapsto \boldsymbol{U}' \subset \boldsymbol{V}'$ defined by

$$a(\underline{\boldsymbol{w}}, \underline{\boldsymbol{z}}) = <\underline{\boldsymbol{w}}, A\underline{\boldsymbol{z}}>, \quad \forall \underline{\boldsymbol{w}} \in \boldsymbol{W},\ \underline{\boldsymbol{z}} \in \boldsymbol{V}.$$

In fact, A is a continuous and invertible operator from $\boldsymbol{V}$ to $\boldsymbol{V}'$ and denote $A^{-1} : \boldsymbol{V}' \mapsto \boldsymbol{V}$.

Let Ω be a bounded domain with $\partial\Omega \in C^3$. Then for any given function $\boldsymbol{f} \in \boldsymbol{V}_h$, we have

$$\|\underline{\boldsymbol{w}}\|_{H^3(\Omega)} \le C\|\boldsymbol{f}\|_{\boldsymbol{V}_h},$$

where $\|\underline{\boldsymbol{w}}\|_{H^3(\Omega)}^2 = \|\boldsymbol{u}\|_{H^3(\Omega_f)}^2 + \|\varphi\|_{H^3(\Omega_p)}^2$. That means

$$\|A^{-1}\boldsymbol{f}\|_{H^3(\Omega)} \le C\|\boldsymbol{f}\|_{\boldsymbol{V}_h}, \quad \forall \boldsymbol{f} \in \boldsymbol{V}_h. \tag{36}$$

From (12), we have

$$a(Q_h\underline{\boldsymbol{w}}, \underline{\boldsymbol{z}}_h) = 0,\ \forall \underline{\boldsymbol{w}} \in \boldsymbol{V},\ \underline{\boldsymbol{z}}_h \in \boldsymbol{V}_h.$$

Considering (13) and (36), we have

$$\|Q_hA^{-1}\underline{\boldsymbol{z}}\|_V \le Ch^2\|A^{-1}\underline{\boldsymbol{z}}\|_{H^3(\Omega)} \le Ch^2\|\underline{\boldsymbol{z}}\|_{\boldsymbol{V}_h}.$$

From the definition of the dual norm, we obtain, for all $\underline{\boldsymbol{w}} \in \boldsymbol{V}$,

$$\begin{aligned}
\|Q_h\underline{\boldsymbol{w}}\|_{\boldsymbol{V}_h'} &= \sup_{\underline{\boldsymbol{z}} \in \boldsymbol{V}_h} \frac{(Q_h\underline{\boldsymbol{w}}, \underline{\boldsymbol{z}})}{\|\underline{\boldsymbol{z}}\|_{\boldsymbol{V}_h}} = \sup_{\underline{\boldsymbol{z}} \in \boldsymbol{V}_h} \frac{(Q_h\underline{\boldsymbol{w}}, AA^{-1}\underline{\boldsymbol{z}})}{\|\underline{\boldsymbol{z}}\|_{\boldsymbol{V}_h}} = \sup_{\underline{\boldsymbol{z}} \in \boldsymbol{V}_h} \frac{a(Q_h\underline{\boldsymbol{w}}, A^{-1}\underline{\boldsymbol{z}})}{\|\underline{\boldsymbol{z}}\|_{\boldsymbol{V}_h}} \\
&= \sup_{\underline{\boldsymbol{z}} \in \boldsymbol{V}_h} \frac{a(Q_h\underline{\boldsymbol{w}}, Q_hA^{-1}\underline{\boldsymbol{z}} + P_h^wA^{-1}\underline{\boldsymbol{z}})}{\|\underline{\boldsymbol{z}}\|_{\boldsymbol{V}_h}} = \sup_{\underline{\boldsymbol{z}} \in \boldsymbol{V}_h} \frac{a(Q_h\underline{\boldsymbol{w}}, Q_hA^{-1}\underline{\boldsymbol{z}})}{\|\underline{\boldsymbol{z}}\|_{\boldsymbol{V}_h}} \\
&\le C \sup_{\underline{\boldsymbol{z}} \in \boldsymbol{V}_h} \frac{\|Q_h\underline{\boldsymbol{w}}\|_V\|Q_hA^{-1}\underline{\boldsymbol{z}}\|_V}{\|\underline{\boldsymbol{z}}\|_{\boldsymbol{V}_h}} \le C \sup_{\underline{\boldsymbol{z}} \in \boldsymbol{V}_h} \frac{h^2\|Q_h\underline{\boldsymbol{w}}\|_V\|\underline{\boldsymbol{z}}\|_{\boldsymbol{V}_h}}{\|\underline{\boldsymbol{z}}\|_{\boldsymbol{V}_h}} = Ch^2\|Q_h\underline{\boldsymbol{w}}\|_V.
\end{aligned} \tag{37}$$

Thus we complete the proof. □

In fact, the proof of the error estimate of the scheme (25) is similar to the process in [21,29,35]. To avoid repetition, we omit the proof and only present the final results.

Lemma 5.2. *Let* $\underline{\boldsymbol{w}}_{1,h}^m = (\boldsymbol{u}_{1,h}^m, \varphi_{1,h}^m)$ *with* $1 \le m \le N$ *be the solution of the first-order scheme (25). Denote* $d_t\underline{\boldsymbol{e}}_1^m = \frac{\underline{\boldsymbol{e}}_1^m - \underline{\boldsymbol{e}}_1^{m-1}}{\Delta t}$. *Under the assumption (10), we have,*

$$\|\underline{\boldsymbol{e}}_1^m\|_0^2 + \Delta t \sum_{n=0}^{m-1} \|\underline{\boldsymbol{e}}_1^{n+1}\|_W^2 \le C\left(\Delta t^2 + h^{2k_1+2} + h^{2k_2+2}\right), \tag{38}$$

$$\|d_t\underline{\boldsymbol{e}}_1^m\|_0^2 + \Delta t \sum_{n=0}^{m-1} \|d_t\underline{\boldsymbol{e}}_1^{n+1}\|_W^2 \le C(\Delta t^2 + h^{2k_1} + h^{2k_2}), \tag{39}$$

where C is a positive constant, which is independent of Δt *and h but dependent of the regularities of the weak solution, and it has different values at different occasions.*

Theorem 5.1. *Let* $\underline{\boldsymbol{w}}_{2,h}^m = (\boldsymbol{u}_{2,h}^m, \varphi_{2,h}^m)$ *with* $1 \le m \le N$ *be the solution of the Para/SDC scheme (29). Under the assumption (10), we have*

$$\|\underline{\boldsymbol{w}}_{2,h}^m - \underline{\boldsymbol{w}}^m\|_0^2 \le C(\Delta t^4 + h^{2k_1+2} + h^{2k_2+2}). \tag{40}$$

where C is a positive constant, which is only dependent of the weak solution.

Proof. Let $(\underline{\boldsymbol{w}}_{1,h}^{n+1}, p_{1,h}^{n+1})$ satisfy (25) and $(\underline{\boldsymbol{w}}_{2,h}^{n+1}, p_{2,h}^{n+1})$ satisfy (29) for $n = 0, \ldots, N-1$. Next we take the average of (6) at time $t = t^n$ and $t = t^{n+1}$: for all $\underline{\boldsymbol{z}} \in \boldsymbol{W}$,

$$\left[\frac{\underline{\boldsymbol{w}}_t^{n+1} + \underline{\boldsymbol{w}}_t^n}{2}, \underline{\boldsymbol{z}}\right] + \frac{1}{2}a(\underline{\boldsymbol{w}}^{n+1} + \underline{\boldsymbol{w}}^n, \underline{\boldsymbol{z}}) + \frac{1}{2}b(\underline{\boldsymbol{z}}, p^{n+1} + p^n) = \left(\frac{\boldsymbol{f}^{n+1} + \boldsymbol{f}^n}{2}, \underline{\boldsymbol{z}}\right).$$

By taking $\underline{z} = \underline{z}_h \in \boldsymbol{W}_h$ in the above equations and $q = q_h \in Q_h$ in the mass conservation equation, simple calculation leads to

$$\begin{cases} \left[\dfrac{\underline{\boldsymbol{w}}^{n+1} - \underline{\boldsymbol{w}}^{n}}{\Delta t}, \underline{z}_h\right] + a\left(\underline{\boldsymbol{w}}^{n+1}, \underline{z}_h\right) + b\left(\underline{z}_h, p^{n+1}\right) = \left[\dfrac{\underline{\boldsymbol{w}}^{n+1} - \underline{\boldsymbol{w}}^{n}}{\Delta t}, \underline{z}_h\right] - \left[\dfrac{\underline{\boldsymbol{w}}_t^{n+1} + \underline{\boldsymbol{w}}_t^{n}}{2}, \underline{z}_h\right] \\ + \dfrac{1}{2}a\left(\underline{\boldsymbol{w}}^{n+1} - \underline{\boldsymbol{w}}^{n}, \underline{z}_h\right) + \dfrac{1}{2}b\left(\underline{z}_h, p^{n+1} - p^{n}\right) + \left(\dfrac{\boldsymbol{f}^{n+1} + \boldsymbol{f}^{n}}{2}, \underline{z}_h\right), \\ b(\underline{\boldsymbol{w}}^{n+1}, q_h) = 0. \end{cases} \tag{41}$$

Subtracting (41) from (29), we have,

$$\begin{cases} \left[\dfrac{\underline{\boldsymbol{e}}_2^{n+1} - \underline{\boldsymbol{e}}_2^{n}}{\Delta t}, \underline{z}_h\right] + a\left(\underline{\boldsymbol{e}}_2^{n+1}, \underline{z}_h\right) + b\left(\underline{z}_h, \varepsilon_2^{n+1}\right) \\ = \left[\dfrac{\underline{\xi}^{n+1} - \underline{\xi}^{n}}{\Delta t}, \underline{z}_h\right] + a\left(\underline{\xi}^{n+1}, \underline{z}_h\right) + b\left(\underline{z}_h, \eta^{n+1}\right) + \left[\dfrac{\underline{\boldsymbol{w}}_t^{n+1} + \underline{\boldsymbol{w}}_t^{n}}{2}, \underline{z}_h\right] - \left[\dfrac{\underline{\boldsymbol{w}}^{n+1} - \underline{\boldsymbol{w}}^{n}}{\Delta t}, \underline{z}_h\right] \\ + \dfrac{1}{2}a\left(\underline{\boldsymbol{w}}_{1,h}^{n+1} - \underline{\boldsymbol{w}}^{n+1}, \underline{z}_h\right) - \dfrac{1}{2}a\left(\underline{\boldsymbol{w}}_{1,h}^{n} - \underline{\boldsymbol{w}}^{n}, \underline{z}_h\right) + \dfrac{1}{2}b\left(\underline{z}_h, p_{1,h}^{n+1} - p^{n+1}\right) - \dfrac{1}{2}b\left(\underline{z}_h, p_{1,h}^{n} - p^{n}\right), \\ b(\underline{\boldsymbol{e}}_2^{n+1}, q_h) = b(\underline{\xi}^{n+1}, q_h) = 0. \end{cases}$$

Take $\underline{z}_h = 2\Delta t\underline{\boldsymbol{e}}_2^{n+1}$ and $q_h = \varepsilon_2^{n+1}$ in the above equations. Notice that $\underline{\boldsymbol{e}}_2^{n+1} \in \boldsymbol{V}_h$. Considering (12) and the decomposition (34), we get

$$\begin{aligned} &a(\underline{\xi}^{n+1}, \underline{\boldsymbol{e}}_2^{n+1}) = b(\underline{\boldsymbol{e}}_2^{n+1}, \eta^{n+1}) = 0, \\ &\quad a(\underline{\boldsymbol{w}}_{1,h}^{n+1} - \underline{\boldsymbol{w}}^{n+1}, \underline{\boldsymbol{e}}_2^{n+1}) - a(\underline{\boldsymbol{w}}_{1,h}^{n} - \underline{\boldsymbol{w}}^{n}, \underline{\boldsymbol{e}}_2^{n+1}) + b(\underline{\boldsymbol{e}}_2^{n+1}, p_{1,h}^{n+1} - p^{n+1}) - b(\underline{\boldsymbol{e}}_2^{n+1}, p_{1,h}^{n} - p^{n}) \\ &= a(\underline{\boldsymbol{e}}_1^{n+1} - \underline{\boldsymbol{e}}_1^{n}, \underline{\boldsymbol{e}}_2^{n+1}) - a(\underline{\xi}^{n+1} - \underline{\xi}^{n}, \underline{\boldsymbol{e}}_2^{n+1}) + b(\underline{\boldsymbol{e}}_2^{n+1}, \varepsilon_1^{n+1} - \varepsilon_1^{n}) + b(\underline{\boldsymbol{e}}_2^{n+1}, \eta^{n+1} - \eta^{n}) \\ &= a(\underline{\boldsymbol{e}}_1^{n+1} - \underline{\boldsymbol{e}}_1^{n}, \underline{\boldsymbol{e}}_2^{n+1}) + b(\underline{\boldsymbol{e}}_2^{n+1}, \varepsilon_1^{n+1} - \varepsilon_1^{n}). \end{aligned}$$

Hence, we can get

$$\begin{aligned} &(\|\underline{\boldsymbol{e}}_2^{n+1}\|_0^2 - \|\underline{\boldsymbol{e}}_2^{n}\|_0^2 + \|\underline{\boldsymbol{e}}_2^{n+1} - \underline{\boldsymbol{e}}_2^{n}\|_0^2) + 2\Delta t\|\underline{\boldsymbol{e}}_2^{n+1}\|_W^2 + 2\Delta t\sum_{i=1}^{d-1}\alpha\sqrt{\frac{\nu g}{\mathrm{tr}(\boldsymbol{K})}}\|\underline{\boldsymbol{e}}_2^{n+1}\cdot\tau_i\|_{L^2(\Gamma)}^2 \\ &\quad \le 2\Delta t\left[\frac{\underline{\xi}^{n+1} - \underline{\xi}^{n}}{\Delta t}, \underline{\boldsymbol{e}}_2^{n+1}\right] + 2\Delta t\left[\frac{\underline{\boldsymbol{w}}_t^{n+1} + \underline{\boldsymbol{w}}_t^{n}}{2} - \frac{\underline{\boldsymbol{w}}^{n+1} - \underline{\boldsymbol{w}}^{n}}{\Delta t}, \underline{\boldsymbol{e}}_2^{n+1}\right] + \Delta t^2 a(d_t\underline{\boldsymbol{e}}_1^{n+1}, \underline{\boldsymbol{e}}_2^{n+1}). \end{aligned} \tag{42}$$

By using the Poincare, Young's inequalities and (9), we get

$$\begin{aligned} &2\Delta t\left[\frac{\underline{\xi}^{n+1} - \underline{\xi}^{n}}{\Delta t}, \underline{\boldsymbol{e}}_2^{n+1}\right] + 2\Delta t\left[\frac{\underline{\boldsymbol{w}}_t^{n+1} + \underline{\boldsymbol{w}}_t^{n}}{2} - \frac{\underline{\boldsymbol{w}}^{n+1} - \underline{\boldsymbol{w}}^{n}}{\Delta t}, \underline{\boldsymbol{e}}_2^{n+1}\right] \\ &\le 2\varepsilon\Delta t\|\underline{\boldsymbol{e}}_2^{n+1}\|_W^2 + \frac{C}{\varepsilon}\Delta t\left\|\frac{\underline{\xi}^{n+1} - \underline{\xi}^{n}}{\Delta t}\right\|_{\boldsymbol{V}_h'}^2 + \frac{C}{\varepsilon}\Delta t\left\|\frac{\underline{\boldsymbol{w}}_t^{n+1} + \underline{\boldsymbol{w}}_t^{n}}{2} - \frac{\underline{\boldsymbol{w}}^{n+1} - \underline{\boldsymbol{w}}^{n}}{\Delta t}\right\|_{W'}^2, \\ &\Delta t^2 a(d_t\underline{\boldsymbol{e}}_1^{n+1}, \underline{\boldsymbol{e}}_2^{n+1}) \le \varepsilon\Delta t\|\underline{\boldsymbol{e}}_2^{n+1}\|_W^2 + \Delta t\sum_{i=1}^{d-1}\alpha\sqrt{\frac{\nu g}{\mathrm{tr}(\boldsymbol{K})}}\|\underline{\boldsymbol{e}}_2^{n+1}\cdot\tau_i\|_{L^2(\Gamma)}^2 + C\Delta t^3\|d_t\underline{\boldsymbol{e}}_1^{n+1}\|_W^2. \end{aligned}$$

Combining the above estimates with (42), choosing $\varepsilon = 1/3$ and summing the error equation (42) from $n = 0$ to $n = m-1$, we obtain

$$\begin{aligned} \|\underline{\boldsymbol{e}}_2^{m}\|_0^2 + \Delta t\sum_{n=0}^{m-1}\|\underline{\boldsymbol{e}}_2^{n+1}\|_W^2 \le \|\underline{\boldsymbol{e}}_2^{0}\|_0^2 + C\Delta t^3\sum_{n=0}^{m-1}\|d_t\underline{\boldsymbol{e}}_1^{n+1}\|_W^2 + C\Delta t\sum_{n=0}^{m-1}\left\|\frac{\underline{\xi}^{n+1} - \underline{\xi}^{n}}{\Delta t}\right\|_{\boldsymbol{V}_h'}^2 \\ + C\Delta t\sum_{n=0}^{m-1}\left\|\frac{\underline{\boldsymbol{w}}_t^{n+1} + \underline{\boldsymbol{w}}_t^{n}}{2} - \frac{\underline{\boldsymbol{w}}^{n+1} - \underline{\boldsymbol{w}}^{n}}{\Delta t}\right\|_{W'}^2. \end{aligned} \tag{43}$$

From (35) and (13), we have

$$\Delta t\sum_{n=0}^{m-1}\left\|\frac{\underline{\boldsymbol{\xi}}_2^{n+1}-\underline{\boldsymbol{\xi}}_2^{n}}{\Delta t}\right\|_{\boldsymbol{V}_h'}^2 \le Ch^4\Delta t\sum_{n=0}^{m-1}\left\|\frac{\underline{\boldsymbol{\xi}}_2^{n+1}-\underline{\boldsymbol{\xi}}_2^{n}}{\Delta t}\right\|_{V}^2 \le Ch^4\sum_{n=0}^{m-1}\int_{t^n}^{t^{n+1}}\|(\underline{\boldsymbol{\xi}}_1)_t\|_V^2\,dt$$
$$\le C(h^{2k_1+2}\|\boldsymbol{u}_t\|^2_{L^2(0,T;H^{k_1}(\Omega_f))}+h^{2k_2+2}\|\varphi_t\|^2_{L^2(0,T;H^{k_2}(\Omega_p))}).$$

From the Taylor expansion, we have,

$$\frac{\underline{\boldsymbol{w}}_t^{n+1}+\underline{\boldsymbol{w}}_t^{n}}{2}-\frac{\underline{\boldsymbol{w}}^{n+1}-\underline{\boldsymbol{w}}^{n}}{\Delta t}=\frac{1}{8}\Delta t^2\underline{\boldsymbol{w}}_{ttt}(\theta_1^n)-\frac{1}{24}\Delta t^2\underline{\boldsymbol{w}}_{ttt}(\theta_2^n),$$

where $\theta_1^n,\ \theta_2^n\in(t^n,t^{n+1})$. Then by using Young's inequality and (10), we obtain

$$\Delta t\sum_{n=0}^{m-1}\left\|\frac{\underline{\boldsymbol{w}}_t^{n+1}+\underline{\boldsymbol{w}}_t^{n}}{2}-\frac{\underline{\boldsymbol{w}}^{n+1}-\underline{\boldsymbol{w}}^{n}}{\Delta t}\right\|_{W'}^2\le C\Delta t^5\sum_{n=0}^{m-1}\sum_{i=1}^{2}\|\underline{\boldsymbol{w}}_{ttt}(\theta_i^n)\|_{W'}^2\le C\Delta t^4\|\underline{\boldsymbol{w}}_{ttt}\|^2_{L^2(0,T;\boldsymbol{W}')}.$$

Combining the above estimates, (39) and (10) with (43), we get

$$\|\underline{\boldsymbol{e}}_2^m\|_0^2+\Delta t\sum_{n=0}^{m-1}\|\underline{\boldsymbol{e}}_2^{n+1}\|_W^2\le C\Big(h^{2k_1+2}\|\boldsymbol{u}_t\|^2_{L^2(0,T;H^{k_1}(\Omega_f))}+h^{2k_2+2}\|\varphi_t\|^2_{L^2(0,T;H^{k_2}(\Omega_p))}\Big)$$
$$+C\Delta t^4\|\underline{\boldsymbol{w}}_{ttt}\|^2_{L^2(0,T;\boldsymbol{W}')}+C\Delta t^2(\Delta t^2+h^{2k_1}+h^{2k_2})$$
$$\le C(\Delta t^4+h^{2k_1+2}+h^{2k_2+2}). \tag{44}$$

Here we use the fact $\underline{\boldsymbol{e}}_2^0=\boldsymbol{0}$. Using the triangle inequality and combining the approximation properties (13) with (44) will lead to the result (40). □

6. Numerical experiments

In this section, we present four numerical experiments to illustrate the accuracy and efficiency of the Para/SDC algorithm. In the first experiment, we compute the convergence orders in time and space for our scheme. The second experiment can illustrate the Para/SDC algorithm is more effective, compared with the serial SDC algorithm. In Experiment 3, we confirm the influence of the errors based on different kinematic viscosity variables ν and hydraulic conductivity variables K. In the last experiment, we change the porous media region Ω_p. Let Ω_p contain a circular region, which can be regarded as a barrier.

The finite element spaces are constructed by using the Mini elements (P_1b-P_1) for the Stokes equations and the piecewise linear Lagrangian elements (P_1) for the Darcy equations. The code was implemented using the software package FreeFem++.

To examine the orders of convergence with respect to the time step and the mesh size, we give a measure of the convergency. If we assume that

$$v_h^{\Delta t}(x,t_m)\approx v(x,t_m)+C_1(x,t_m)\Delta t^{\gamma}+C_2(x,t_m)h^{\mu},$$

the measures testing the convergence order of the time step Δt and the mesh size h are defined as follows:

$$\rho_{v,h,0}=\frac{\|\,v_h^{\Delta t}(x,t_m)-v_{\frac{h}{2}}^{\Delta t}(x,t_m)\,\|_0}{\|\,v_{\frac{h}{2}}^{\Delta t}(x,t_m)-v_{\frac{h}{4}}^{\Delta t}(x,t_m)\,\|_0}\approx\frac{4^{\mu}-2^{\mu}}{2^{\mu}-1},$$
$$\rho_{v,\Delta t,0}=\frac{\|\,v_h^{\Delta t}(x,t_m)-v_h^{\frac{\Delta t}{2}}(x,t_m)\,\|_0}{\|\,v_h^{\frac{\Delta t}{2}}(x,t_m)-v_h^{\frac{\Delta t}{4}}(x,t_m)\,\|_0}\approx\frac{4^{\gamma}-2^{\gamma}}{2^{\gamma}-1}. \tag{45}$$

Here v can be $\boldsymbol{u}$ or φ. While $\rho_{v,\,\Delta t,\,0}$ and $\rho_{v,\,h,\,0}$ approach 4.0, the convergence order will be 2.0.

6.1. Experiment 1

Let the computational domain be $\Omega_f=[0,1]\times[1,2]$, $\Omega_p=[0,1]\times[0,1]$ and the interface $\Gamma=(0,1)\times\{1\}$. The exact solutions of the mixed Stokes/Darcy equations are given by

$$\boldsymbol{u}(x,y,t)=(x^2(y-1)^2+y)\cos(t),\Big(-\frac{2}{3}x(y-1)^3+2-\pi\sin(\pi x)\Big)\cos(t)),$$
$$p(x,y,t)=\big(2-\pi\sin(\pi x)\big)\sin\Big(\frac{\pi}{2}y\Big)\cos(t), \tag{46}$$
$$\varphi(x,y,t)=\big(2-\pi\sin(\pi x)\big)\big(1-y-\cos(\pi y)\big)\cos(t)+\frac{1}{2}\big(1+(2-\pi\sin(\pi x))^2\big)\big((y-1)^2+1\big)\cos^2(t).$$

In this experiments, we set the physical parameters $\nu=1$, $S_0=1$, $g=1$, $\alpha=1$ and the hydraulic conductivity tensor $\boldsymbol{K}=K\boldsymbol{I}$, where the hydraulic conductivity variable $K=1$. We verify the convergence order of the time step Δt by fixing

Table 1
The convergence orders of the Para/SDC scheme at time $t_m = 1$, with the fixed mesh $h = 1/8$ and varying time step Δt.

Δt	$\|\boldsymbol{u}^m_{2,\Delta t} - \boldsymbol{u}^m_{2,\frac{\Delta t}{2}}\|_{L^2(\Omega_f)}$	$\rho_{\boldsymbol{u},\Delta t,0}$	$\|\varphi^m_{2,\Delta t} - \varphi^m_{2,\frac{\Delta t}{2}}\|_{L^2(\Omega_p)}$	$\rho_{\varphi,\Delta t,0}$
1/20	7.16288e-6	3.93034	1.52583e-4	3.97619
1/40	1.82246e-6	3.96607	3.83742e-5	3.99290
1/80	4.59513e-7	3.98326	9.61062e-6	3.99760
1/160	1.15361e-7	3.99167	2.40410e-6	3.99904
1/320	2.89004e-8		6.01169e-7	

Table 2
The convergence orders of the Para/SDC scheme at time $t_m = 1$, with the fixed time step $\Delta t = 1/20$ and the varying mesh step h.

h	$\|\boldsymbol{u}^m_{2,h} - \boldsymbol{u}^m_{2,\frac{h}{2}}\|_{L^2(\Omega_f)}$	$\rho_{\boldsymbol{u},h,0}$	$\|\varphi^m_{2,h} - \varphi^m_{2,\frac{h}{2}}\|_{L^2(\Omega_p)}$	$\rho_{\varphi,h,0}$
1/2	2.08537e-1	3.96482	4.32668e-1	3.63797
1/4	5.25969e-2	4.01515	1.18931e-1	3.96985
1/8	1.30996e-2	4.03839	2.99586e-2	3.86706
1/16	3.24377e-3	3.77312	7.74713e-3	4.17768
1/32	8.59705e-4		1.85441e-3,	

Table 3
The CPU time of the Para/SDC scheme and the serial SDC scheme with the fixed mesh $h = 1/00$.

Method	CPU			
	$\Delta t = 1/10$	$\Delta t = 1/20$	$\Delta t = 1/40$	$\Delta t = 1/80$
SDC	80.263	161.841	321.787	649.848
Para/SDC	37.487	98.233	128.146	250.343

Table 4
The convergence orders of the Para/SDC scheme at time $t_m = 1$, with the fixed mesh $h = 1/8$ and varying time step Δt.

Δt	$\nu = 10^{-1}$				$\nu = 10^{-5}$			
	$\|\boldsymbol{e}^m_u\|_{0,\Omega_f}$	$\rho_{\boldsymbol{u},\Delta t,0}$	$\|\boldsymbol{e}^m_\varphi\|_{0,\Omega_p}$	$\rho_{\varphi,\Delta t,0}$	$\|\boldsymbol{e}^m_u\|_{0,\Omega_f}$	$\rho_{\boldsymbol{u},\Delta t,0}$	$\|\boldsymbol{e}^m_\varphi\|_{0,\Omega_p}$	$\rho_{\varphi,\Delta t,0}$
1/10	8.39097e-5	3.54240	5.95016e-4	3.91033	5.76385e-4	3.94825	5.64573e-4	3.89734
1/20	2.36873e-5	3.74592	1.52165e-4	3.97398	1.45985e-4	3.96335	1.44861e-4	3.95650
1/40	6.32350e-6	3.86583	3.82903e-5	3.99145	3.68337e-5	3.94290	3.66134e-5	3.95646
1/80	1.63574e-6	3.91926	9.59307e-6	3.99641	9.34179e-6	3.81980	9.25407e-6	3.92574
1/160	4.17359e-7		2.40042e-6		2.44562e-6		2.35728e-6	

the mesh size $h = 1/8$ and setting varying time steps $\Delta t = 1/20,\ 1/40,\ 1/80,\ 1/160,\ 1/320$. These results in Table 1 indicate that the Para/SDC method is second-order accurate. A series of $\rho_{\boldsymbol{u},h,0}$ and $\rho_{\varphi,h,0}$ are listed in Table 2 with fixed time step $\Delta t = 1/20$ and varying spacing h, which clearly suggests that the convergence order in space is optimal. All data in Tables 1 and 2 are consistent with the theoretical analysis in Theorem 5.1.

6.2. Experiment 2

In order to verify the effectiveness, we design an experiment to compare the CPU time of the Para/SDC algorithm with that of the serial second-order SDC algorithm. We set the parameters the same as Experiment 1. The results are list in Table 3. Obviously, our scheme indeed costs less CPU time than the serial SDC algorithm.

6.3. Experiment 3

In this experiment, we confirm the influence of the errors based on different kinematic viscosity variables ν and hydraulic conductivity variables K. For simplicity, we denote that $\|\boldsymbol{e}^m_u\|_{0,\Omega_f} = \|\boldsymbol{u}^m_{2,\Delta t} - \boldsymbol{u}^m_{2,\frac{\Delta t}{2}}\|_{L^2(\Omega_f)}$ and $\|\boldsymbol{e}^m_\varphi\|_{0,\Omega_p} = \|\varphi^m_{2,\Delta t} - \varphi^m_{2,\frac{\Delta t}{2}}\|_{L^2(\Omega_p)}$. Firstly, we calculate the convergence order in time, showing that the numerical solutions still satisfy the second order of convergence, see Tables 4 and 5. Secondly, we compare the errors between the numerical solutions and the exact solutions. The results of Table 6 show that the errors for the fluid velocity $\boldsymbol{u}$ increase as kinematic viscosity variables ν decreases. In Table 7, we choose different hydraulic conductivity variables K, the results suppose to show that the values of hydraulic conductivity variables have a greater effect on the piezometric head φ.

Table 5
The convergence orders of the Para/SDC scheme at time $t_m = 1$, with the fixed mesh $h = 1/8$ and varying time step Δt.

Δt	$K = 0.1$				$K = 0.01$			
	$\|\boldsymbol{e}_u^m\|_{0,\Omega_f}$	$\rho_{\boldsymbol{u},\Delta t,0}$	$\|\boldsymbol{e}_\varphi^m\|_{0,\Omega_p}$	$\rho_{\varphi,\Delta t,0}$	$\|\boldsymbol{e}_u^m\|_{0,\Omega_f}$	$\rho_{\boldsymbol{u},\Delta t,0}$	$\|\boldsymbol{e}_\varphi^m\|_{0,\Omega_p}$	$\rho_{\varphi,\Delta t,0}$
1/10	3.61669e-4	4.41748	1.50600e-2	4.21788	1.62462e-4	3.86432	3.70852e-2	3.84365
1/20	8.18722e-5	4.21630	3.57051e-3	4.06416	4.20416e-5	3.88580	9.64844e-3	3.90764
1/40	1.94180e-5	4.09289	8.78536e-4	3.99649	1.08193e-5	3.86162	2.46912e-3	3.93833
1/80	4.74433e-6	4.01871	2.19827e-4	3.94772	2.80175e-6	3.76683	6.26946e-4	3.94036
1/160	1.18056e-6		5.56845e-5		7.43795e-7		1.59109e-4	

Table 6
The error for the Para/SDC scheme at time $t_m = 1$, with fixed $h = 1/100$, $\Delta t = 1/2$ and $K = 1$.

Δt	$\nu = 1$	$\nu = 10^{-1}$	$\nu = 10^{-3}$	$\nu = 10^{-5}$
$\|\boldsymbol{u}_{2,h}^m - \boldsymbol{u}^m\|_{L^2(\Omega_)}$	1.26596e-3	1.51331e-2	5.00160e-1	8.12845e-1
$\|\varphi_{2,h}^m - \varphi^m\|_{L^2(\Omega_p)}$	1.33681e-2	1.36715e-2	5.19811e-2	7.97252e-2

Table 7
The error for the Para/SDC scheme at time $t_m = 1$, with fixed $h = 1/100$, $\Delta t = 1/2$ and $\nu = 1$.

Δt	$K = 1$	$K = 0.1$	$K = 0.01$	$K = 0.001$
$\|\boldsymbol{u}_{2,h}^m - \boldsymbol{u}^m\|_{L^2(\Omega_)}$	1.26596e-3	7.41861e-2	2.24906e-1	3.29615e-1
$\|\varphi_{2,h}^m - \varphi^m\|_{L^2(\Omega_p)}$	1.33681e-2	1.16589e+1	3.58247e+1	5.71824e+1

Table 8
The convergence orders of the Para/SDC scheme at time $t_m = 1$, with the fixed mesh $h = 1/8$ and varying time step Δt.

Δt	$\|\boldsymbol{u}_{2,\Delta t}^m - \boldsymbol{u}_{2,\frac{\Delta t}{2}}^m\|_{L^2(\Omega_f)}$	$\rho_{\boldsymbol{u},\Delta t,0}$	$\|\varphi_{2,\Delta t}^m - \varphi_{2,\frac{\Delta t}{2}}^m\|_{L^2(\Omega_p)}$	$\rho_{\varphi,\Delta t,0}$
1/10	2.92310e-5	3.85357	1.64231e-4	4.05235
1/20	7.58544e-6	3.93131	4.05274e-5	4.04051
1/40	1.92949e-6	3.96667	1.00303e-5	4.02387
1/80	4.86426e-7	3.98359	2.49269e-6	4.01285
1/160	1.22107e-7		6.21177e-7	

6.4. Experiment 4

Set the porous region $\Omega_p = \Omega_p'/D$ where $\Omega_p = [0,1] \times [0,1]$ and D is the circle with the radiu 0.2cm and the dot (0.5,0.5). The fluid domain still is $\Omega_f = [0,1] \times [1,2]$ and the interface $\Gamma = (0,1) \times \{1\}$. Note again we set the physical parameters $\nu = 1$, $S_0 = 1$, $g = 1$, $\alpha = 1$ and $\boldsymbol{K} = K\boldsymbol{I}$ with $K = 1$. The results in Table 8 shows that the convergence order of the time step is still second order.

7. Conclusion

In this paper, we present a second-order Para/SDC algorithm for the non-stationary mixed Stokes/Darcy equations with the BJS interface condition. The numerical stability and the optimal error estimate are presented. And the numerical experiments demonstrate the effectiveness of our scheme.

References

[1] J.L. Lions, Y. Maday, G. Turinici, A "parareal" in time discretization of pde's, C. R. Acad. Sci. Ser. I-Math. 332 (7) (2001) 661–668.
[2] G.A. Staff, E.M. Rønquist, Stability of the Parareal Algorithm, Springer, Berlin Heidelberg, 2005.
[3] M.J. Gander, E. Hairer, Nonlinear Convergence Analysis for the Parareal Algorithm, Springer, Berlin Heidelberg, 2008.
[4] M.J. Gander, S. Vandewalle, On the superlinear and linear convergence of the parareal algorithm, Domain Decomposition Methods in Science and Engineering XVI, vol. 55, Springer Berlin Heidelberg, 2007, pp. 291–298.
[5] G. Bal, On the convergence and the stability of the parareal algorithm to solve partial differential equations, Domain Decomposition Methods in Science and Engineering, Springer Berlin Heidelberg, 2005, pp. 425–432.
[6] Y. Maday, The parareal in time algorithm, Substructuring Techniques and Domain Decomposition Methods, Saxe-Coburg Publications, Stirling, UK, 2010, pp. 19–44.
[7] E. Aubanel, Scheduling of tasks in the parareal algorithm, Parallel Comput. 37 (3) (2011) 172–182.
[8] P.F. Fischer, F. Hecht, Y. Maday, A Parareal in Time Semi-implicit Approximation of the Navier-Stokes Equations, Springer, Berlin Heidelberg, 2005.
[9] C. Farhat, J. Cortial, C. Dastillung, H. Bavestrello, Time-parallel implicit integrators for the near-real-time prediction of linear structural dynamic responses, Int. J. Numer. Methods Eng. 67 (5) (2010) 697–724.
[10] E. Celledoni, T. Kvamsdal, Parallelization in time for thermo-viscoplastic problems in extrusion of aluminium, Int. J. Numer. Methods Eng. 79 (5) (2010) 576–598.
[11] S. Bu, J.Y. Lee, An enhanced parareal algorithm based on the deferred correction methods for a stiff system, J. Comput. Appl. Math. 255 (285) (2014) 297–305.

[12] M.J. Gander, M. Petcu, Analysis of a Krylov subspace enhanced parareal algorithm for linear problems, ESAIM Proc. 25 (2) (2008) 114–129.
[13] M.L. Minion, S.A. Williams, Parareal and spectral deferred corrections, AIP Conf. Proc. 1048 (1) (2008) 388–391.
[14] M.L. Minion, A hybrid parareal spectral deferred corrections method, Commun. Appl. Math. Comput. Sci. 5 (5) (2011) 265–301.
[15] A. Dutt, L. Greengard, V. Rokhlin, Spectral deferred correction methods for ordinary differential equations, Bit Numer. Math. 40 (2) (2000) 241–266.
[16] M.L. Minion, Semi-implicit projection methods for incompressible flow based on spectral deferred corrections, Appl. Numer. Math. 48 (3) (2004) 369–387.
[17] M.L. Minion, Semi-implicit spectral deferred correction methods for ordinary differential equations, Commun. Math. Sci. 1 (3) (2002) 2127–2157.
[18] A. Bourlioux, A.T. Layton, M.L. Minion, High-order multi-implicit spectral deferred correction methods for problems of reactive flow, J. Comput. Phys. 189 (2) (2003) 651–675.
[19] P. Hessari, B.C. Shin, First order system least squares pseudo-spectral method for Stokes–Darcy equations, Appl. Numer. Math. 120 (2017) 35–52.
[20] W.J. Layton, F. Schieweck, I. Yotov, Coupling fluid flow with porous media flow, SIAM J. Numer. Anal. 40 (6) (2002) 2195–2218.
[21] M. Mu, X. Zhu, Decoupled schemes for a non-stationary mixed stokes-darcy model, Math Comput 79 (270) (2010) 707–731.
[22] Y. Mabrouki, S.M. Aouadi, J. Satouri, Spectral discretization of Darcy equations coupled with stokes equations by vorticity-velocity-pressure formulations: spectral discretization of darcy-stokes equations, Numer. Methods Partial Differ. Equ. 33 (2017) 1628–1651.
[23] Y. Cao, M. Gunzburger, X. Hu, F. Hua, X. Wang, W. Zhao, Finite element approximations for Stokes–Darcy flow with Beavers–Joseph interface conditions, SIAM J Numer Anal 47 (6) (2014) 4239–4256.
[24] M. Mu, J. Xu, A two-grid method of a mixed Stokes–Darcy model for coupling fluid flow with porous media flow, SIAM J. Numer. Anal. 45 (5) (2007) 1801–1813.
[25] Y. Hou, Optimal error estimates of a decoupled scheme based on two-grid finite element for mixed Stokes–Darcy model, Appl. Math. Lett. 57 (2016) 90–96.
[26] W. Feng, X. He, Z. Wang, X. Zhang, Non-iterative domain decomposition methods for a non-stationary Stokes–Darcy model with Beavers–Joseph interface condition, Appl. Math. Comput. 219 (2) (2012) 453–463.
[27] G. Fu, C. Lehrenfeld, A strongly conservative hybrid DG/mixed FEM for the coupling of stokes and Darcy flow, J. Sci. Comput. 77 (3) (2018) 1605–1620.
[28] C. Bernardi, A.Y. Orfi, A priori error analysis of the fully discretized time-dependent coupled Darcy and stokes equations, SeMa J. 38 (3) (2004) 1–23.
[29] L. Shan, H. Zheng, W.J. Layton, A decoupling method with different subdomain time steps for the nonstationary Stokes–Darcy models, Numer. Methods Partial Differ. Equ. 29 (2) (2013) 549–583.
[30] V. Girault, G. Kanschat, B. Rivire, Error analysis for a monolithic discretization of coupled Darcy and stokes problems, J. Numer. Math. 22 (2) (2014) 109–142.
[31] Z. Si, Y. Wang, S. Li, Decoupled modified characteristics finite element method for the time dependent Navier–Stokes/Darcy problem, Math. Methods Appl. Sci. 37 (9) (2014) 1392–1404.
[32] Y. Wang, S. Li, Z. Si, A second order in time incremental pressure correction finite method method for the Navier–Stokes/Darcy problem, ESAIM Math. Modell. Numer. Anal. 52 (4) (2017) 1477–1500.
[33] G. Beavers, D. Joseph, Boundary conditions at a naturally permeable wall, J. Fluid Mech. 30 (1967) 197–207.
[34] P. Saffman, On the boundary condition at the surface of a porous medium, Stud. Appl. Math. 50 (1971) 93–101.
[35] Y. Rong, Y. Hou, Y. Zhang, Numerical analysis of a second order algorithm for simplified magnetohydrodynamic flows, Adv. Comput. Math. 43 (4) (2017) 823–848.